Gate-Tunable Topological Flat Bands in Trilayer Graphene Boron-Nitride Moiré Superlattices

Bheema Lingam Chittari,[1,2] Guorui Chen,[2] Yuanbo Zhang,[3,4] Feng Wang,[2] and Jeil Jung[1,2,*]
[1]Department of Physics, University of Seoul, Seoul 02504, Korea
[2]Department of Physics, University of California at Berkeley, Berkeley, California 94709, USA
[3]State Key Laboratory of Surface Physics and Department of Physics, Fudan University, Shanghai 200433, China
[4]Institute for Nanoelectronic Devices and Quantum Computing, Fudan University, Shanghai 200433, China

(Received 1 June 2018; published 3 January 2019)

We investigate the electronic structure of the flat bands induced by moiré superlattices and electric fields in nearly aligned *ABC* trilayer graphene (TLG) boron-nitride (BN) interfaces where Coulomb effects can lead to correlated gapped phases. Our calculations indicate that valley-spin resolved isolated superlattice flat bands that carry a finite Chern number $C = 3$ proportional to the layer number can appear near charge neutrality for appropriate perpendicular electric fields and twist angles. When the degeneracy of the bands is lifted by Coulomb interactions, these topological bands can lead to anomalous quantum Hall phases that embody orbital and spin magnetism. Narrow bandwidths of ∼10 meV achievable for a continuous range of twist angles $\theta \lesssim 0.6°$ with moderate interlayer potential differences of ∼50 meV make the TLG-BN systems a promising platform for the study of electric-field tunable Coulomb-interaction-driven spontaneous Hall phases.

DOI: 10.1103/PhysRevLett.122.016401

The generation of moiré superlattices in graphene and other 2D materials by forming van der Waals interfaces has emerged as an efficient route to tailor high-quality artificial band structures [1–3]. In particular, the periodic moiré patterns in the length scale of a few tens of nanometers that arise due to a small lattice constant mismatch or twist angles with the substrate give rise to moiré mini-Brillouin zones whose zone corners are at energy ranges accessible by conventional field effects in gated transistor devices [4–10]. The interlayer coupling becomes effectively strong in the limit of long moiré pattern periods due to nonperturbative coupling between the superlattice zone folded moiré bands [4,5], which suggests that flat bands can routinely form in the limit of long moiré pattern periods for a variety of 2D material combinations including twisted bilayer graphene and transition metal dichalcogenide heterojunctions [11–13]. Recent experiments have shown resistance peaks as a function of carrier doping indicative of Mott phases in twisted bilayer graphene at the first magic twist angle [14,15] and in *ABC* trilayer graphene (TLG) nearly aligned with hexagonal boron nitride (BN) [16] when the Fermi energy is brought near the superlattice flat bands (SFBs). In this Letter, we carry out an analysis of the SFBs in TLG-BN, showing that they are generally topological bands; i.e., they have finite Chern numbers, and the lifting of the valley-spin degeneracy by Coulomb-interaction-driven gaps of these Chern flat bands (CFBs) can give rise to quantum anomalous Hall phases with orbital and spin magnetism even in the absence of an external magnetic field.

Model Hamiltonian.—The model Hamiltonian for *ABC* stacked TLG is based on the low-energy model for trilayer graphene with the band parameters obtained from density functional theory local density approximation (LDA) [17–19]. We represent the Hamiltonian acting in the basis of the low-energy sites A for bottom and B for top layers. Each band is fourfold degenerate, with twofold degeneracy in the principal valleys (K, K'), labeled with $\nu = \pm 1$, and twofold degeneracy in real spin $(\uparrow, \downarrow)$, labeled with $s = \pm 1$. We label the lowest valence and conduction (h, e) bands through $b = \pm 1$. The low-energy Hamiltonian for a rhombohedral N-layer graphene is

$$H_N^{\nu,\xi} = \frac{v_0^N}{(-t_1)^{N-1}} \begin{pmatrix} 0 & (\pi^\dagger)^N \\ \pi^N & 0 \end{pmatrix} + \Delta\sigma_z + H_N^R + H_\xi^M, \quad (1)$$

where $\pi = (\nu p_x + i p_y)$. We will discuss our results for the $\nu = 1$ principal valley K unless stated otherwise. The parameter Δ represents an adjustable interlayer potential difference between the top and bottom layers that include the effects of a perpendicular electric field and its screening. In a TLG with $N = 3$ layers, we model the remote hopping-term corrections through

$$H_{3,\nu}^R = \left[\left(\frac{2v_0v_3p^2}{t_1} + t_2\right)\sigma_x\right] + \left[\frac{2v_0v_4p^2}{t_1} - \Delta' + \Delta''\left(1 - \frac{3v_0^2p^2}{t_1^2}\right)\right]\mathbb{1}. \quad (2)$$

 © 2019 American Physical Society

The effective hopping parameters are $t_0 = -2.62$ eV, $t_1 = 0.358$ eV, $t_2 = -0.0083$ eV, $t_3 = 0.293$ eV, and $t_4 = -0.144$ eV [19,20], where the associated velocities are defined as $v_m = \sqrt{3}a|t_m|/2\hbar$, with $a = 2.46$ Å being the lattice constant of graphene. The diagonal terms $\Delta' = 0.0122$ eV and $\Delta'' = 0.0095$ eV are used to provide an accurate fit for the LDA bands. The moiré patterns have a period $\ell_M \simeq a/(\varepsilon^2 + \theta)^{1/2}$ that depends on $\varepsilon = (a - a_{BN})/a_{BN}$, the relative lattice constant mismatch between graphene and BN, and the twist angle θ. The moiré potential generated in graphene due to BN is given by

$$H^M_{\xi=\pm1}(\vec{r}) = V^M_{A/B}(\vec{r}) = 2C_{A/B}\mathrm{Re}[e^{i\phi_{A/B}} f(\vec{r})]\frac{(\xi\sigma_z + \mathbb{1})}{2}, \tag{3}$$

where the moiré parameters are $C_A = -14.88$ meV, $\phi_A = 50.19°$ and $C_B = 12.09$ meV, $\phi_B = -46.64°$ [4,21], and the auxiliary function $f(\vec{r}) = \sum_{m=1}^{6} e^{i\vec{G}_m\cdot\vec{r}}[1 + (-1)^m]/2$ is expressed using the six moiré reciprocal lattices $\vec{G}_{m=1\ldots6} = \hat{R}_{2\pi(m-1)/3}\vec{G}_1$ successively rotated by sixty degrees, where $\vec{G}_1 = [0, 4\pi/(\sqrt{3}\ell_M)]$. Two possible alignment potentials between TLG and BN, labeled by $\xi = \pm1$, that perturb the low-energy A (bottom) or B (top) sites in graphene contacting BN give rise to different band structures.

Topological flat bands in TLG-BN superlattices.—The presence of moiré superlattices can produce avoided gaps at the moiré mini-Brillouin-zone (mBZ) boundaries [22–24], while an additional gap at the primary Dirac point would isolate the low-energy bands near charge neutrality [16,21,25,26]. Because the low-energy bands in *ABC* trilayers are less dispersive than those of single or bilayer graphene, they are particularly suitable for the efficient isolation and narrowing of the low-energy bands by electric fields that enhance both the primary and secondary gaps [16]. Here, we discuss how the gaps opened by perpendicular electric fields lead to Berry curvatures in the isolated flat bands of TLG-BN and can turn them into topological Chern bands with a quantized Hall effect. The Berry curvature for the nth band can be calculated using the standard formula $\Omega_n(\vec{k}) = -2\sum_{n'\neq n}\mathrm{Im}[\langle u_n|(\partial H/\partial k_x)|u_{n'}\rangle\langle u_{n'}|\partial H/\partial k_y|u_n\rangle/(E_{n'} - E_n)^2]$ [27], where for every k point we take sums through all the neighboring n' bands, the $|u_n\rangle$'s are the moiré superlattice Bloch states, and the E_n's are the eigenvalues. The Chern number of the nth band $C = C_{\nu,s,N,\xi,b}$ calculated through $C = \int_{\mathrm{mBZ}} d^2\vec{k}\Omega_n(\vec{k})/(2\pi)$ assumes implicit indices. In Fig. 1, we can observe the Berry curvature hot spots near the primary and secondary gaps with larger Chern number weights.

Our numerical calculations for TLG-BN predict the Chern numbers $C = \pm3$ for the CFBs depending on system parameters. We have verified up to trilayers that

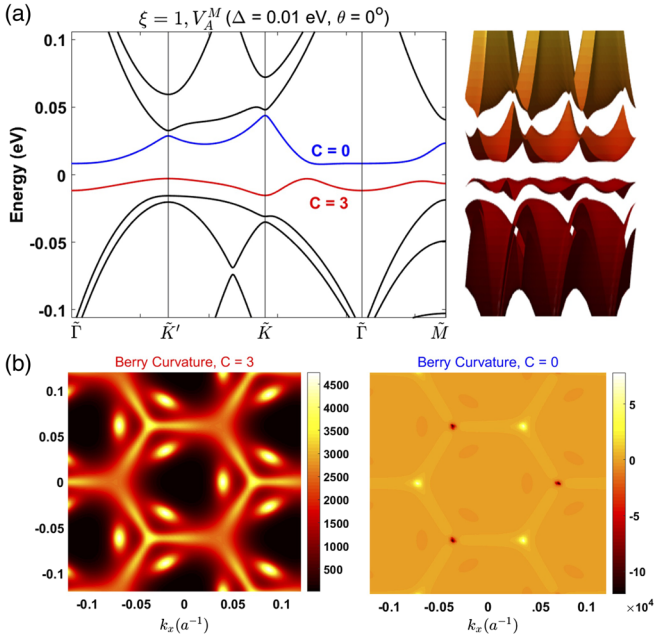

FIG. 1. (a) The band structure of ABC-TLG for zero twist angle near charge neutrality in the folded zones representation subject to $V_A^M = H_{\xi=1}^M$ moiré patterns and interlayer potential differences of $\Delta = 10$ meV that give rise to flat Chern bands, with $C = 3$ represented in red and the trivial $C = 0$ band represented in blue. (b) The Berry curvatures for the valence and conduction band structures of panel (a), where we see Berry curvature hot spots near the trigonal warping band edges and mBZ boundaries that add up in the Chern band. In the trivial band, we see sharp peaks with opposite Berry curvatures, mainly at the mBZ boundaries, that cancel out.

$$C = N\nu\xi\delta_{\mathrm{sgn}(\Delta)\cdot\xi,b} \tag{4}$$

in an N-chiral graphene two-dimensional electron gas (2DEG), where the Chern bands are found for either the valence or conduction bands depending on applied electric field sign and moiré pattern potential. In Fig. 2, we show that the calculated Chern numbers are quantized for a wide range of Δ values for valence and conduction bands of TLG-BN and BLG-BN. In particular, we find that either the conduction or valence SFB near charge neutrality becomes a Chern band as soon as Δ opens a gap at the primary Dirac point. This behavior can be understood if we consider that a rhombohedral N-layer graphene [28] develops in the limit of small Δ a primary Chern weight $w_P \sim \mathrm{sgn}(\Delta)b\nu N/2$ near each valley whose sign depends on $\mathrm{sgn}(\Delta)$ and the hole or electron band character $b = \pm1$, as well as the valley $\nu = \pm1$ [29–32]. In the absence of secondary gaps due to moire patterns, the K and K' principal valleys are mutually connected, and the valley Chern numbers identified as Chern weights w_P near each valley are not protected topological numbers. Nevertheless, they give an intuitive idea about the Hall conductivity dynamics near the chiral 2DEG band edges and are useful for

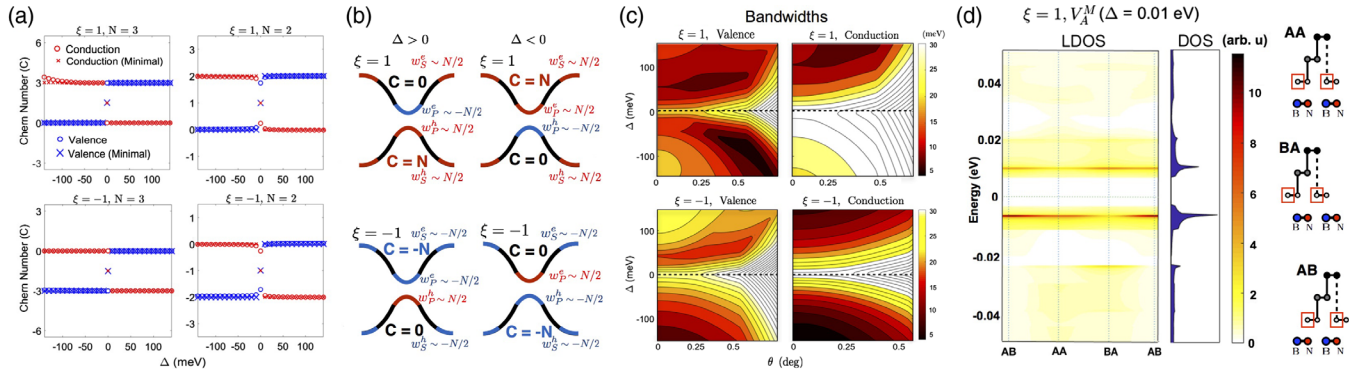

FIG. 2. (a) Chern numbers for the valence and conduction flat bands for aligned TLG on BN for the bands in Eqs. (1) and (2), bilayer on BN using H_2^R from Ref. [20], and corresponding minimal $H_\xi^R = 0$ models, calculated using a total of 18 361 k points in the mBZ. An abrupt transition happens when the sign of Δ changes near zero field. (b) Schematic illustration of the Chern weights near $\tilde{\Gamma}$ and the mBZ boundaries in the limit of $|\Delta| \ll 1$ that add up into an integer $C^{e/h} = w_P^{e/h} + w_S^{e/h}$, where $w_P^e = -w_P^h$ and $w_S^e = w_S^h$, so that either the electron or hole band has a finite Chern number. (c) Bandwidth phase diagram for the valence and conduction bands as a function of interlayer potential difference Δ and twist angle θ calculated from the difference between the maximum and minimum eigenvalue within a band. (d) Local stacking and energy-dependent LDOS and DOS manifesting the localization of flatband wave functions.

counting the number of zero-line modes in the valley Hall domain walls [31–38]. The situation is quite different when primary and secondary gaps are simultaneously present near the mBZ boundaries, because the Chern weights sum $C^{e/h} = w_P^{e/h} + w_S^{e/h}$ needs to add up to a zero or finite integer value in each isolated band [39], where w_S^e and w_S^h are the secondary Chern weights for the electron and hole bands. The value s of $w_S^{e/h}$ depends on the moiré pattern that generates the avoided secondary gaps, as evidenced by the fact that different moiré potentials V_A^M or V_B^M give rise to flat bands with different Chern numbers. The abrupt change in the band Chern number with the sign of Δ can be related with the sign changes of w_P. Considering that $w_P^h = -w_P^e$ for electrons and holes in the limit $|\Delta| \ll 1$, we conclude that the secondary weights should initially be equal, $w_S^e = w_S^h$ (see Fig. 2), while unequal electron-hole secondary Chern weights $w_S^e \neq w_S^h$ might be achievable using different moiré and Hamiltonian parameters. For increasing Δ, the primary Chern weights are progressively pushed from the vicinity of $\tilde{\Gamma}$ towards the mBZ boundaries closer to the location of the secondary weights $w_S^{e/h}$ while maintaining a constant Chern number in the isolated bands. Conclusions similar to our analysis in TLG-BN could be expected in other rhombohedral multilayer graphene N-chiral 2DEGs, although the remote hopping terms in the band Hamitonian are important to properly account for the flatband dispersions and the secondary gaps. Figures S1 and S2 in the Supplemental Material illustrate the Chern weights in the mBZ from small to large Δ in minimal N-chiral multilayer graphene with $N = 1, 2, 3$ [40].

Field-dependent bandwidths and localization.—The external electric field strength modulates the size of the primary band gap near $\tilde{\Gamma}$, which impacts directly the shape of the low-energy SFBs, and their optimum flatness will depend on field direction and strength. In Fig. 2, we represent a color map that summarizes the evolution of the bandwidth of the SFBs as a function of electric field and twist angle quantified through the difference between the maximum and minimum energy values within a given band. We can observe that for every given twist angle, there is often an optimum interlayer potential difference that maximizes the band flatness for either positive or negative field directions, highlighting the electron-hole asymmetry inherent in TLG-BN, and that the overall flatness does not always grow monotonically with increasing electric field magnitude. Increasing Δ to appropriately large values will favor the onset of Coulomb-interaction-driven gaps by increasing the separation of the SFBs with neighboring energy bands and reducing their bandwidth. The parameter space of Δ and θ where $U_{\text{eff}}/W \gtrsim 1$ is favorable for the onset of ordered phases can be found in Fig. S4 in the Supplemental Material [40]. In addition to the electric field magnitude and direction, the relative twist angle in the system has an impact in the flatness and energy location of the SFBs. Introducing a finite twist angle is expected to widen the moiré bands due to the increase in the size of the mBZ in reciprocal space for reduced moiré real-space periods. However, for relatively small twist angle values of up to ∼1°, the moiré pattern periods are still ∼10 nm, and the enhanced suppression of achievable bandwidth through external electric fields can sufficiently compensate for this bandwidth increase due to rotation. Direct information on the band flatness is reflected in the density of states (DOS) plots as a function of energy allowing us to find the energy regions where Coulomb correlations are expected to be stronger. The local density of states (LDOS) plots for every local stacking configuration also provide insights on the electron localization properties of the SFB electrons in real space; see Fig. 2. Charge and spin density modulations are

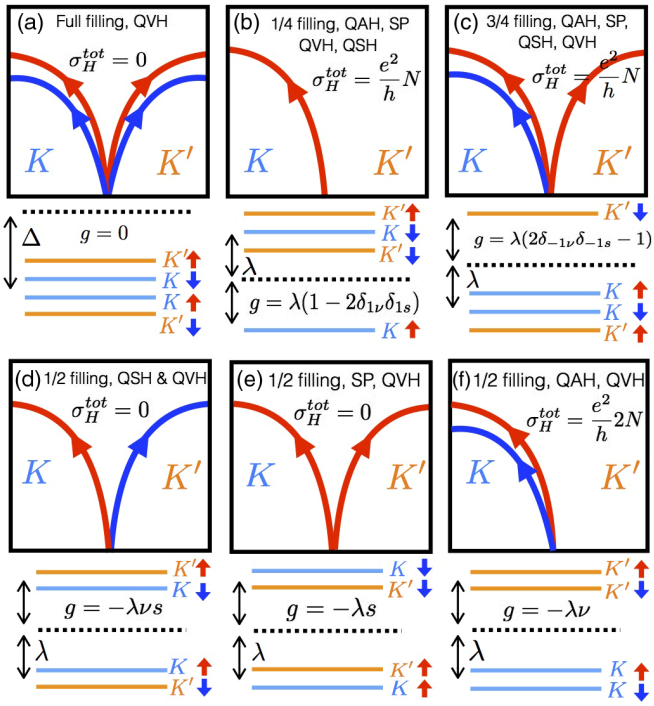

FIG. 3. For the valence flat bands associated with $\Delta > 0$ and $\xi = 1$ moiré potentials, we schematically represent how the occupation of valley $\nu = (K, K')$ and spin $s = (\uparrow, \downarrow)$ resolved CFBs contributes towards the generation of orbital and spin magnetism of different signs. Different band occupations can be pictured by shifting the band energies by a $g(\nu, s)$ function. Four different configurations of valley spin are possible for (b) 1/4 and (c) 3/4 fillings, and two for each 1/2 filling represented in (d)–(f). The total charge Hall conductivity $\sigma_H^{\rm tot} = \sum_i \sigma_H^i$ of the bands is contributed by $\sigma_H^i = C_i e^2/h$ for each occupied valley-spin flavor i, where $C_i = N\nu\xi\delta_{{\rm sgn}(\Delta)\cdot\xi,b}$, and the valley Hall conductivity is proportional to filling. A variety of spontaneous quantum anomalous, valley, and spin Hall effects should be expected when interaction-driven gaps open for 1/4, 1/2, and 3/4 fillings of the CFB. In particular, 1/4 and 3/4 fillings are found to simultaneously have spin and orbital magnetism.

expected to take place mainly around the LDOS peaks when the degeneracy of the bands is lifted due to Coulomb interactions. The LDOS plots provide valuable information for guiding scanning probe microscopy experiments that search for flatband signatures.

Spontaneous quantum Hall phases.—Filling of nontrivial Chern bands will lead to an associated quantum Hall effect that should be observable in transport experiments. An interesting scenario is found in partially filled CFB when valley and spin degeneracy is lifted by Coulomb interactions, giving rise to a variety of spontaneous quantum Hall phases. We take as a working assumption that the interaction-driven gapped states at 1/4, 1/2, and 3/4 partial fillings of the flat bands will develop into spin-collinear and valley-collinear phases, where each valley-spin flavor can be filled sequentially. In the Hartree-Fock approximation, it is reasonable to assume that the same spin polarization will

TABLE I. Summary of the Chern flatband configurations (1 for occupied, 0 for unoccupied) and corresponding charge, spin, and valley Hall conductivities (in e^2/h units) and insulator types: Quantum anomalous Hall (QAH), spin Hall (QSH), valley Hall (QVH), and spin polarized (SP). The layer number $N = 3$ is equal to the flatband Chern number magnitude in TLG-BN.

Fig.	$K\uparrow$	$K\downarrow$	$K'\uparrow$	$K'\downarrow$	$\sigma^{(\rm CH)}$	$\sigma^{(\rm SH)}$	$\sigma^{(\rm VH)}$	Insulator
3(a)	1	1	1	1	0	0	$4N$	QVH
3(b)	1	0	0	0	N	0	N	QAH, SP, QVH
3(c)	1	1	1	0	N	$-N$	$3N$	QAH, QSH, SP, QVH
3(d)	1	0	0	1	0	$2N$	$2N$	QSH, QVH
3(e)	1	0	1	0	0	0	$2N$	SP, QVH
3(f)	1	1	0	0	$2N$	0	$2N$	QAH, QVH

be preferred over noncollinear spin states as in conventional quantum Hall ferromagnetism of Landau levels [41], while valley polarized phases can be preferred due to momentum space exchange condensation over valley-coherent phases with two partially filled valleys [42]. We represent Coulomb-interaction-driven gaps through rigid shifts proportional to λ in the CFB energies through a function $g(\nu, s)$ to classify the different possible states assuming any of them are possible. We will follow a classification scheme closely similar to the four valley-spin components of N-chiral multilayer graphene in Refs. [30,43], in our case facilitated by the fact that the quantum valley Hall effect is proportional to CFB filling. In Fig. 3, we illustrate for the example of the $b = 1$, $\xi = 1$, $\Delta > 0$ case corresponding to the top panel of Fig. 1 a representative selection of quantum Hall ground states, also summarized in Table I. At charge neutrality, when all CFBs are filled to filling 1, we have a valley Hall state where the charge Hall conductivity summed over all occupied flavors totals to zero, and the charge Hall conductivity is $\sigma_H^{\rm tot} = \sum_i \sigma_H^i = 0$. The cases of 1/4 and 3/4 fillings can be pictured through the selective filling and emptying of a given (ν', s') band using shifts of $g(\nu, s) = \lambda(1 - 2\delta_{\nu'\nu}\delta_{s's})$ and $\lambda(2\delta_{\nu'\nu}\delta_{s's} - 1)$, respectively. These are interesting cases with $\sigma_H^{\rm tot} = \pm Ne^2/h$ charge Hall conductivity, where we have simultaneously a quantum anomalous and spin Hall effect. For the 1/2 filling, when two CFBs are filled, we have a greater variety of quantum Hall ground states. One of the possibilities is the quantum anomalous Hall phase where two equal ν' valley CFBs are filled. The shift functions can then be modeled through $g(\nu, s) = \lambda(1 - 2\delta_{\nu'\nu})$, and the charge Hall conductivity is $\sigma_H^{\rm tot} = 2N\nu' e^2/h$. The remaining two scenarios have Hall conductivity $\sigma_H^{\rm tot} = 0$, in the case where the same spin s' are polarized and are modeled through $g(\nu, s) = \lambda(1 - 2\delta_{s's})$ shifts, and the quantum spin phase can be modeled through $g(\nu, s) = \pm\lambda\nu s$ shifts depending on the relative signs of the occupied valley-spin indices.

Discussions.—In this Letter, we have analyzed the topological character of the superlattice flat bands (SFBs) in *ABC* trilayer graphene-hexagonal boron-nitride

superlattices, where signatures of gate-tunable Mott gaps have been observed recently in experiments [16]. Our analysis indicates that topological flat bands with Chern number $C = \pm 3$ will form either for electrons or for holes depending on the electric field sign and moiré potential. This scenario makes it possible to study Coulomb-interaction-driven ordered phases in zero and finite Chern number flat bands within the same device by modifying the carrier density from electrons to holes, making this system an interesting platform for exploring the interplay of correlation physics with topological order. Band gap openings for partial filling of the flat bands indicate that a selective occupation of Chern flat bands (CFBs) of different valley-spin flavors should be possible. Assuming valley-spin collinear ground states of these partially filled CFBs, different types of spontaneous quantum Hall phases with orbital and spin magnetization can be expected, with total charge Hall conductivities of zero or $\sigma_H^{\mathrm{tot}} = \pm 6e^2/h$ expected for 1/2 filling, whereas $\sigma_H^{\mathrm{tot}} = \pm 3e^2/h$ that is always finite is expected for 1/4 or 3/4 fillings. From a device application point of view, one important advantage of the field-tunable gapped Dirac materials is that the bandwidth variations of the SFBs are less sensitive to twist angle compared to twisted bilayer graphene, where a precise twist angle control is required.

We thank A. H. MacDonald for helpful discussions. B. L. C. was supported by the Basic Science Research Program through the National Research Foundation of Korea (NRF) funded by the Ministry of Education (No. 2018R1A6A1A06024977) and by Grants No. NRF-2016R1A2B4010105 and No. NRF-2017R1D1A1B03035932. G. C. and F. W. acknowledge the support of the Director, Office of Science, Office of Basic Energy Sciences, Materials Sciences and Engineering Division of the U.S. Department of Energy under Contract No. DE-AC02-05-CH11231 (van der Waals heterostructures program, KCWF16). Y. Z. acknowledges financial support from the National Key Research Program of China (Grants No. 2016YFA0300703 and No. 2018YFA0305600), the NSF of China (Grants No. U1732274, No. 11527805, No. 11425415, and No. 11421404), the Shanghai Municipal Science and Technology Commission (Grant No. 18JC1410300), and the Strategic Priority Research Program of the Chinese Academy of Sciences (Grant No. XDB30000000). J. J. was supported by the Samsung Science and Technology Foundation under Project No. SSTF-BA1802-06.

Note added.—A recent related work is Ref. [44].

*jeiljung@uos.ac.kr

[1] B. Hunt, J. D. Sanchez-Yamagishi, A. F. Young, M. Yankowitz, B. J. LeRoy, K. Watanabe, T. Taniguchi, P. Moon, M. Koshino, P. Jarillo-Herrero, and R. C. Ashoori, Science **340**, 1427 (2013).
[2] C. R. Dean, L. Wang, P. Maher, C. Forsythe, F. Ghahari, Y. Gao, J. Katoch, M. Ishigami, P. Moon, M. Koshino, T. Taniguchi, K. Watanabe, K. L. Shepard, J. Hone, and P. Kim, Nature (London) **497**, 598 (2013).
[3] L. A. Ponomarenko, R. V. Gorbachev, G. L. Yu, D. C. Elias, R. Jalil, A. A. Patel, A. Mishchenko, A. S. Mayorov, C. R. Woods, J. R. Wallbank, M. Mucha-Kruczynski, B. A. Piot, M. Potemski, I. V. Grigorieva, K. S. Novoselov, F. Guinea, V. I. Fal'ko, and A. K. Geim, Nature (London) **497**, 594 (2013).
[4] J. Jung, A. Raoux, Z. Qiao, and A. H. MacDonald, Phys. Rev. B **89**, 205414 (2014).
[5] R. Bistritzer and A. H. MacDonald, Proc. Natl. Acad. Sci. U.S.A. **108**, 12233 (2011).
[6] G. Li, A. Luican, J. L. Dos Santos, A. C. Neto, A. Reina, J. Kong, and E. Andrei, Nat. Phys. **6**, 109 (2010).
[7] J. R. Wallbank, A. A. Patel, M. Mucha-Kruczynski, A. K. Geim, and V. I. Fal'ko, Phys. Rev. B **87**, 245408 (2013).
[8] J. M. B. Lopes dos Santos, N. M. R. Peres, and A. H. Castro Neto, Phys. Rev. Lett. **99**, 256802 (2007).
[9] P. Moon and M. Koshino, Phys. Rev. B **85**, 195458 (2012).
[10] M. Yankowitz, J. Xue, D. Cormode, J. D. Sanchez-Yamagishi, K. Watanabe, T. Taniguchi, P. Jarillo-Herrero, P. Jacquod, and B. J. LeRoy, Nat. Phys. **8**, 382 (2012).
[11] F. Wu, T. Lovorn, E. Tutuc, and A. H. MacDonald, Phys. Rev. Lett. **121**, 026402 (2018).
[12] Y. Pan, S. Folsch, Y. Nie, D. Waters, Y.-C. Lin, B. Jariwala, K. Zhang, K. Cho, J. A. Robinson, and R. M. Feenstra, Nano Lett. **18**, 1849 (2018).
[13] S. Carr, D. Massatt, M. Luskin, and E. Kaxiras, arXiv:1803.01242.
[14] Y. Cao, V. Fatemi, A. Demir, S. Fang, S. L. Tomarken, J. Y. Luo, J. D. Sanchez-Yamagishi, K. Watanabe, T. Taniguchi, E. Kaxiras, R. C. Ashoori, and P. Jarillo-Herrero, Nature (London) **556**, 80 (2018).
[15] Y. Cao, V. Fatemi, S. Fang, K. Watanabe, T. Taniguchi, E. Kaxiras, and P. Jarillo-Herrero, Nature (London) **556**, 43 (2018).
[16] G. Chen, L. Jiang, S. Wu, B. Lv, H. Li, K. Watanabe, T. Taniguchi, Z. Shi, Y. Zhang, and F. Wang, arXiv:1803.01985.
[17] F. Zhang, B. Sahu, H. Min, and A. H. MacDonald, Phys. Rev. B **82**, 035409 (2010).
[18] M. Koshino and E. McCann, Phys. Rev. B **80**, 165409 (2009).
[19] J. Jung *et al.* (to be published).
[20] J. Jung and A. H. MacDonald, Phys. Rev. B **89**, 035405 (2014).
[21] J. Jung, A. M. DaSilva, A. H. MacDonald, and S. Adam, Nat. Commun. **6**, 6308 (2015).
[22] J. Jung, E. Laksono, A. M. DaSilva, A. H. MacDonald, M. Mucha-Kruczynski, and S. Adam, Phys. Rev. B **96**, 085442 (2017).
[23] A. M. DaSilva, J. Jung, S. Adam, and A. H. MacDonald, Phys. Rev. B **91**, 245422 (2015).
[24] E. Wang *et al.*, Nat. Phys. **12**, 1111 (2016).

[25] J. C. W. Song, P. Samutpraphoot, and L. S. Levitov, Proc. Natl. Acad. Sci. U.S.A. **112**, 10879 (2015).
[26] P. San-Jose, A. Gutiérrez-Rubio, M. Sturla, and F. Guinea, Phys. Rev. B **90**, 115152 (2014).
[27] D. Xiao, M.-C. Chang, and Q. Niu, Rev. Mod. Phys. **82**, 1959 (2010).
[28] H. Min and A. H. MacDonald, Prog. Theor. Phys. Suppl. **176**, 227 (2008).
[29] D. Xiao, W. Yao, and Q. Niu, Phys. Rev. Lett. **99**, 236809 (2007).
[30] F. Zhang, J. Jung, G. A. Fiete, Q. Niu, and A. H. MacDonald, Phys. Rev. Lett. **106**, 156801 (2011).
[31] J. Jung, F. Zhang, Z. Qiao, and A. H. MacDonald, Phys. Rev. B **84**, 075418 (2011).
[32] J. Jung, Z. Qiao, Q. Niu, and A. H. MacDonald, Nano Lett. **12**, 2936 (2012).
[33] G. E. Volovik, *The Universe in a Helium Droplet*, International Series of Monographs on Physics Vol. 117 (Oxford University Press, Oxford, 2009).
[34] I. Martin, Y. M. Blanter, and A. F. Morpurgo, Phys. Rev. Lett. **100**, 036804 (2008).
[35] C. Lee, G. Kim, J. Jung, and H. Min, Phys. Rev. B **94**, 125438 (2016).
[36] J. Li, K. Wang, K. J. McFaul, Z. Zern, Y. Ren, K. Watanabe, T. Taniguchi, Z. Qiao, and J. Zhu, Nat. Nanotechnol. **11**, 1060 (2016).
[37] F. Zhang, A. H. MacDonald, and E. Mele, Proc. Natl. Acad. Sci. U.S.A. **110**, 10546 (2013).
[38] L. Ju, Z. Shi, N. Nair, Y. Lv, C. Jin, J. Velasco, Jr., C. Ojeda-Aristizabal, H. A. Bechtel, M. C. Martin, A. Zettl, J. Analytis, and F. Wang, Nature (London) **520**, 650 (2015).
[39] M. Z. Hasan and C. L. Kane, Rev. Mod. Phys. **82**, 3045 (2010).
[40] See Supplemental Material at http://link.aps.org/supplemental/10.1103/PhysRevLett.122.016401 for band structures and Berry curvatures of the minimal band Hamiltonian for trilayer, bilayer, and monolayer graphene on boron-nitride, and the phase diagram of U_{eff}/W ratio as a function of system parameters Δ and θ.
[41] *The Quantum Hall Effect*, edited by R. E. Prange and S. M. Girvin, 2nd ed. (Springer, Berlin, 1990).
[42] J. Jung, M. Polini, and A. H. MacDonald, Phys. Rev. B **91**, 155423 (2015).
[43] J. Jung, F. Zhang, and A. H. MacDonald, Phys. Rev. B **83**, 115408 (2011).
[44] Y.-H. Zhang, D. Mao, Y. Cao, P. Jarillo-Herrero, and T. Senthil, arXiv:1805.08232.